Int J Earth Sci (Geol Rundsch) (2007) 96:887–902
DOI 10.1007/s00531-006-0142-2

ORIGINAL PAPER

Geological, geochemical and mineralogical features of some bauxite deposits from Nurra (Western Sardinia, Italy): insights on conditions of formation and parental affinity

Paola Mameli · Giovanni Mongelli · Giacomo Oggiano · Enrico Dinelli

Received: 28 June 2005 / Accepted: 18 October 2006 / Published online: 2 December 2006

Abstract Bauxite deposits are widespread in NW Sardinia. They formed during the middle Cretaceous, in consequence of a period of emergence of the Mesozoic carbonate shelf. In the Nurra area the geometries derived by the Middle Cretaceous tectonic phases controlled the ore typologies. Two bauxite profiles, laying on different bedrocks, were sampled. The bauxitization proceeded from the surface downward, with the accumulation of Al_2O_3 and residual 'immobile' elements (Al, Ti, HFSE), and corresponding mobility and loss of SiO_2 and Fe_2O_3. Epigenetic kaolinite formed close to faults and joints, probably as a result of silicification, introduced by low temperature hydrothermal solutions. Rare earth elements, especially LREE, are concentrated in Fe-rich bauxite horizons, probably due to scavenging by goethite. REE-enrichment is not observed in the boehmite-rich horizons. Very high REE contents are observed in a Fe-depleted horizon due to the occurrence of REE accessory minerals, probably of the bastnäsite group. Conservative indices, including TiO_2/Al_2O_3 and Ti/Cr ratios, and Eu anomalies (Eu/Eu*), suggest that the deposits formed by weathering of sediments derived from mafic rocks of the Hercynian basement. This, in turn, implies that the basement was exposed during middle Cretaceous.

Keywords Bauxite · Weathering · Fe oxy-hydroxides · REE · Sardinia

P. Mameli (✉) · G. Oggiano
Istituto di Scienze Geologico-Mineralogiche,
Università degli Studi di Sassari,
Corso Angioj 10, Sassari 07100, Italy
e-mail: mamelip@uniss.it

G. Mongelli
Dipartimento di Scienze Geologiche,
Università degli Studi della Basilicata,
Campus di Macchia Romana, Potenza 85100, Italy

E. Dinelli
Dipartimento di Scienze della Terra e
Geologico-Ambientali, Università degli Studi di Bologna,
Piazza di Porta S. Donato, Bologna 40126, Italy

Introduction

Bauxite deposits can be classified into two main categories, depending on the bedrock lithology: bauxite deposits overlying alumosilicate rocks and bauxite deposits overlying carbonate rocks. According to Bardossy (1982), bauxite overlying alumosilicate rocks can be further subdivided into: (1) laterite bauxites that consist of residual deposits and/or deposits that experienced only local redeposition; and (2) Tikhvin-type bauxites, represented by transported (allochthonous) deposits without any relationship with the original residual profile. Bauxite lying on carbonate rocks can be identified with the 'karstic' category, regardless of whether the bedrock surface is karstified or not, or the degree of karstification.

Karst bauxites, representing 14% of world bauxite resources, have, in turn, been subdivided into several types (Combes 1972; Bardossy 1982 and references therein), based on morphology, composition and geographical–paleogeographical criteria. Among the various types of karst bauxite, the Mediterranean-type is the most widely studied. A wide variety of deposits' subtypes have been distinguished based on different criteria. The subdivision of Bardossy (1982) is based

either on geometrical or compositional features. Other subdivisions (Combes 1972, 1990; Laville 1981; Oggiano et al. 1987) take tectonic setting, allochtony of the lateritic products and the vertical evolution of the chemical and mineralogical profile into consideration.

Mediterranean-type bauxites were generated on both the European and Adriatic Mesozoic carbonate shelves in the Neotethys realm. In Western Europe, this kind of bauxite occurs in the Pyrenean–Provençal domain, where periodic emergences of the carbonate shelf, under favourable climatic conditions, allowed lateritic weathering. The carbonate shelf of western Sardinia, which was part of this domain, experienced a relatively long period of emergence in the middle Cretaceous due to a phase of tectonic instability. Emergence and erosion must have taken place under a warm and wet climate. During the middle Cretaceous, Sardinia lay close to N30° latitude at the same palaeoclimatic belt as the south European margin (Dercourt et al. 1985). Moreover a global warming is recorded during the Albian that caused globally higher temperatures than today (Frakes 1979, 1986) and monsoonal climate in the Pyrenean domain (Fenner 2001; Herrle et al. 2003). Such climate allowed extreme weathering conditions, forming bauxite deposits (Pecorini 1965). At Nurra the deposits display the main features of karst bauxite situated in intracontinental zones. Combes et al. (1993) distinguished three different types of deposit according to the nature of the bedrock. In particular, stratiform deposits sandwiched between Coniacian limestones and Valanginian marls can also form. This is the case of the 'Sardinia-type' deposit (Combes 1990), which is considered an explicit example of a continuous profile of residual bauxite derived from marls.

Although fractionation of major, minor and trace elements occurs during bauxitization, the distribution of immobile elements has proven to be a powerful tool in assessing the genetic history of karst bauxite deposits in the Mediterranean area (e.g., Maksimovic and Pantò 1991; MacLean et al. 1997; Mongelli 1997). The distribution of rare earth elements (REE) in Apulian karst bauxites, for example, permitted assessment of relevant geochemical changes during bauxitization (Mongelli 1997). In addition, conservative elemental indices, such as the Eu/Eu* index, were used to model the parental affinity (Morelli et al. 2000).

This study focuses on two different types of deposit from the Nurra district (western Sardinia) and aims to

1. better define the relationships between the middle Cretaceous tectonics of western Sardinia and the typology of the different deposits;
2. give new constraints on the condition of bauxite formation focusing on the 'mobility' of major and selected trace elements, including rare earth (REE), high field strength elements (HFSE) and transition elements in bauxite samples from different types of deposit from the Nurra district;
3. better constrain the evolution of Nurra bauxites during and after bauxitization, and to determine the source of the ancestor material.

The new data could be of broad interest for further comparisons between bauxites of the Europe and Adria plates. Moreover they can represent a new tool useful in prospecting for new profitable deposits.

Geological setting

The Nurra bauxites are hosted within the Mesozoic carbonate platform of NW Sardinia (Fig. 1). In this region, most of the Variscan basement is capped by a sedimentary sequence which reflects the geodynamic evolution from the collapse of the Variscan orogenic chain to the onset of Neo-Tethyan rifting in the late Triassic. Between the Late Permian and Oligocene, Nurra experienced the same Mesozoic events as other areas of southern stable Europe bounding the passive margin of the Ligure–Piemontese oceanic domain. Accordingly, it was only marginally involved in the Alpine orogeny. In fact the Corsica–Sardinia block was located along the southern edge of stable Europe, close to Provence, before its Neogene counter-clockwise rotation (Vigliotti and Langenheim 1995).

Shallow marine sedimentation of evaporites and carbonates occurred during the long period of tectonic quiescence from the Middle Triassic to the middle Cretaceous. The shelf sea covered the entire post-Variscan peneplain of Sardinia in the Middle Jurassic. The first tectonic activity to affect the Mesozoic carbonate shelf occurred during the middle Cretaceous. This is recognized as low-angle angular unconformities, including a bauxite-bearing stratigraphic hiatus between the Early and Late Cretaceous successions (Fig. 2). This tectonic event was chiefly a sinistral strike-slip motion between the Iberian and European plates. The early movements were characterized by transtensional kinematics that started in the Aptian and lasted until the middle Albian (Bedoulian movements; Rousset 1969). Since the upper Albian, the kinematics turned into transpressional, due to convergence between Iberia and Europe (Puigdefabregas and Souquet 1986). In NW Sardinia, as well as in Provence,

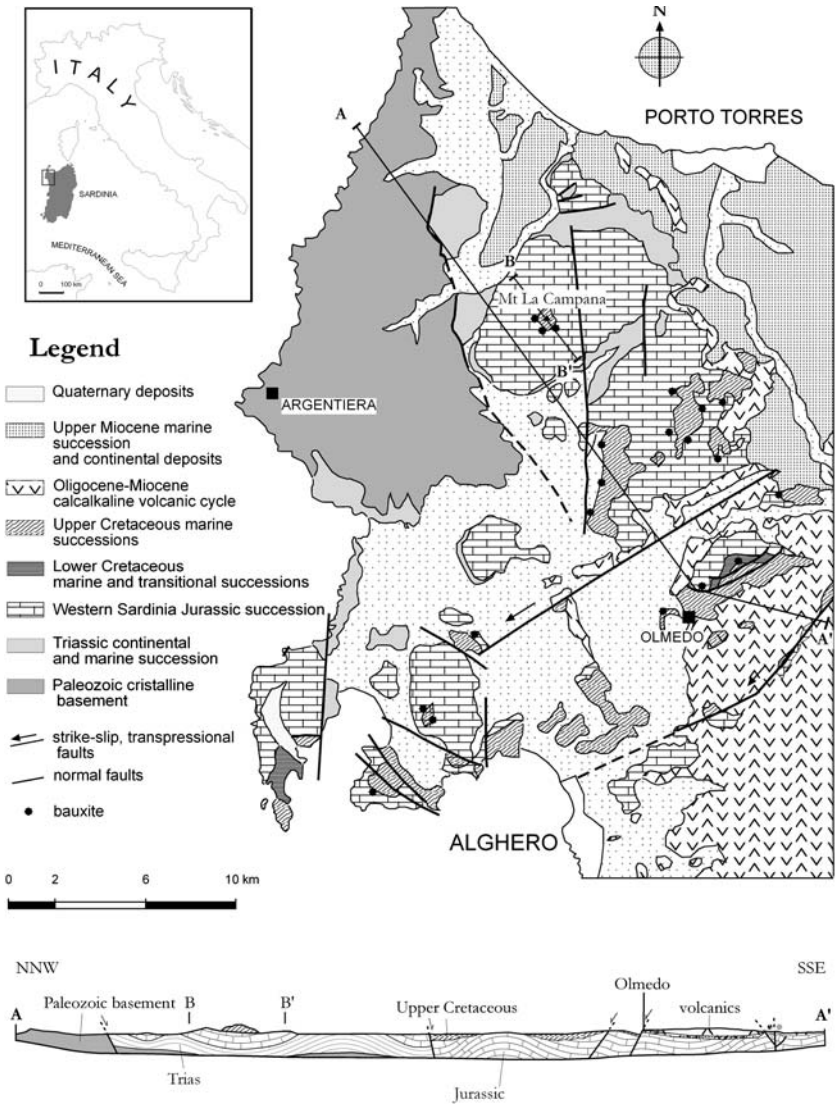

Fig. 1 Geological map of the Nurra region showing the bauxite outcrops below the Upper Cretaceous marine successions. Cross section gives an idea of the continuity of the bauxitic units

middle Cretaceous emergence was related to these later transpressional movements, which generated uplifted blocks and wide antiformal and synformal structures (Oggiano et al. 1987; Combes 1990; Combes et al. 1993). As a consequence during the planation of the mid-Cretaceous surface different rocks of different age were exposed to weathering, depending on the structural frame issued from the Aptian deformation phase. Broadly, the older rocks underlying the bauxite were exposed north-westward (bauxite lying on Dogger dolostones at La Campana) due to the erosive elision of at least 600 m of Mesozoic sequence (Fig. 1). Moving farther in that direction even the entire Mesozoic carbonate platform might have been eroded leading to the exposition of the Palaeozoic basement. Pre–upper Cretaceous erosion of the Mesozoic covers is well documented in northern-central Sardinia where upper Cretaceous carbonate rests directly on Triassic deposits and on basement rocks (Cherchi and Schroeder 1976).

Conversely the younger strata below the bauxite are exposed to ENE and to WSW (Lower Aptian at Uri and Capo Caccia, respectively). Locally folds with different length-waves are also detectable. For example near Olmedo the bauxite and the upper Cretaceous beds seal a wide NNW trending syncline bearing Purbeckian marls and early Barremian limestone in the core (Fig. 3).

The Mesozoic succession, which predates middle Cretaceous emergence, is well exposed at Nurra. It consists mainly of pure dolostones and limestones, with clay-rich beds occurring within the Triassic deposits as marly limestones, and clayey gypsum deposits. Marls also occur in the Late Jurassic strata and, particularly at the base of the Cretaceous, with typical lagoonal-lacustrine 'Purbeckian' facies (Pecorini 1969). Due to

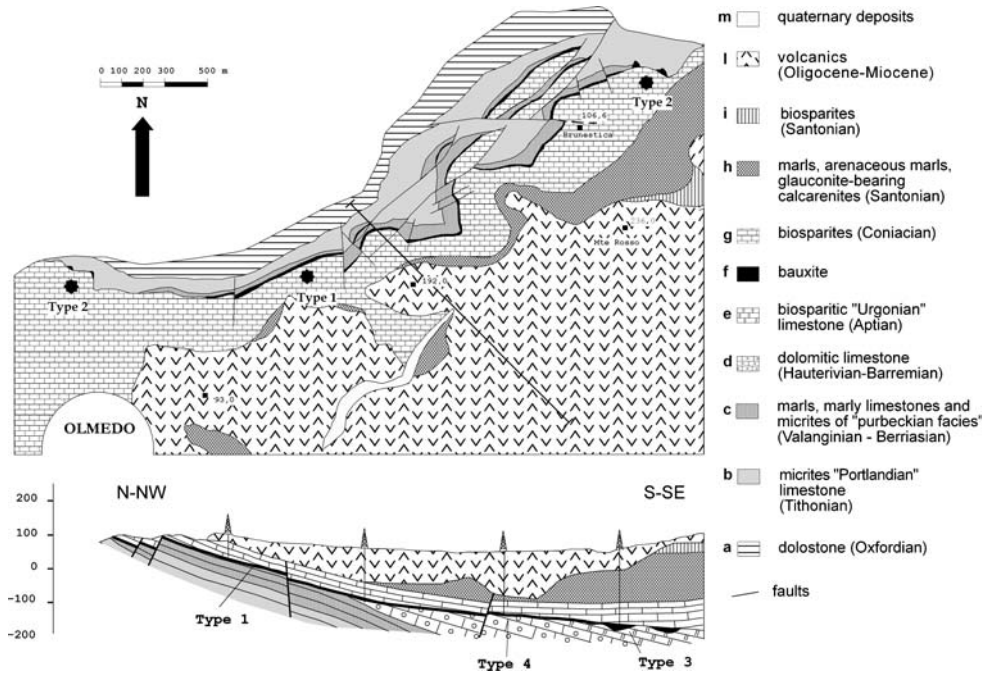

Fig. 2 Geological map and cross section of the mined area of Olmedo. The different Types of bauxite deposits are evidenced both in the map and in the cross section

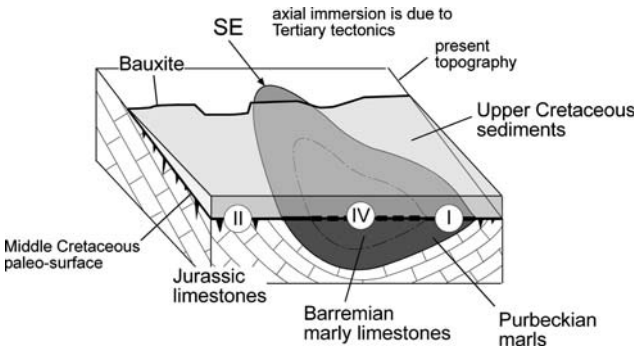

Fig. 3 Example of structural control of pre-upper Cretaceous tectonics on the bauxite deposits: a wide syncline sealed by bauxite and transgressive Coniacian limestone (Olmedo mine)

the angular unconformities noted previously, the bauxite rests on rocks with different compositions, including pure Urgonian limestones, Purbeckian marls and more or less marly limestones and dolostones. The bedrock lithologies control the morphology and the profiles of the bauxite deposits.

The bauxite is covered by transgressive, *Hippurites*-bearing, limestones and marls of Late Cretaceous age (Coniacian to Maastrichtian), which are in turn unconformably capped by pyroclastic products related to the Oligocene–Miocene calc-alkaline volcanic suite of western Sardinia. Open folds, related to a Late Cretaceous or Eocene Pyrenaic tectonic phase, affect the entire Mesozoic sequences along with Neogene normal faults. The Cenozoic deformative phases overprint the middle Cretaceous structures and are responsible for the present distribution of the deposits.

Deposit types

According to Combes (1990) and Combes et al. (1993), marls or other Al_2O_3-rich parent rocks give rise to in situ profiles, whereas on pure limestone or dolostone the bauxite profile derives from more or less weathered material which, following erosion and transport across shorter or longer distances, can be redeposited within structural depressions or inside narrow karsts. These resedimented materials may then undergo further alteration (relative autochthony) or not (allochthony). Combes et al. (1993) divided the Nurra deposits into three different types. Considering an additional type, introduced in the present contribution, the deposits of the Nurra can be subdivided as follows (Fig. 4):

Type-1: regular, stratiform, residual deposits (autochthonous) These are deposits with wide lateral continuity, generally 2 m, with maximum of 5 m, in thickness. The bauxite was derived from *in situ* lateritization of illitic marls (Purbeckian facies). The profile consists of clayey bauxite near the footwall, which grades upwards to a lithic boehmite bauxite, with low hematite and goethite contents. The Fe-minerals are confined to irregular reddish patches within totally bleached ore. Kaolinite is confined to the lower, clay-rich horizon and progressively diminishes toward the

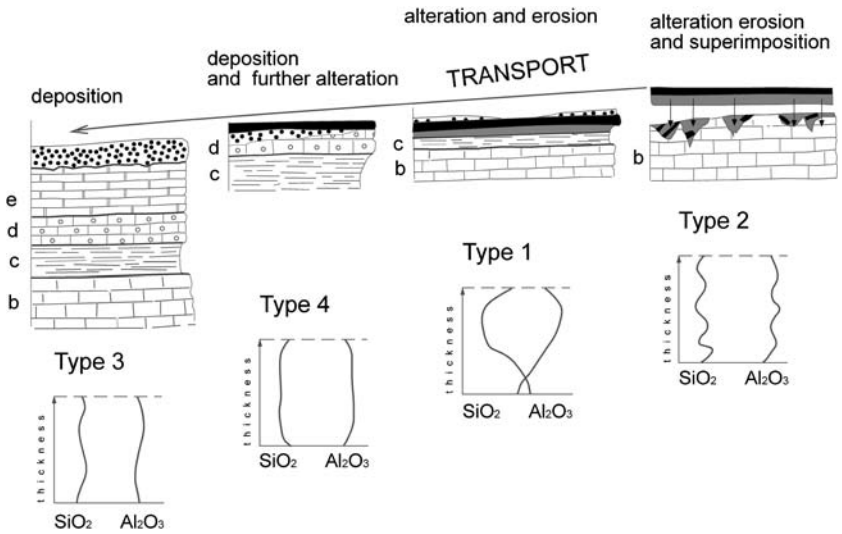

Fig. 4 Tectonic control on different ore deposits typology (modified after Combes at al. 1993). Schematic distribution of both Al_2O_3 and SiO_2 along the different profiles are showed *below*

centre of the deposit, where the Al_2O_3 content can exceed 70%. The abundance of kaolinite increases again in the upper part of the deposit where detrital bauxite can form the uppermost horizon.

Type-2: Karst pockets Bauxite and bauxitic clay infill karsts developed on calcareous or dolomitic beds underlying the Purbeckian marls. They are derived from the Type-1 bauxite profile collapsed into karst pockets hosted in Late Jurassic rocks. These deposits have scarce economic relevance due to the occurrence of clays and bauxitic clays at different levels through the profile.

Type-3: detrital deposits These deposits are uncommon and rest on post-Berriasian bedrock, i.e., on Urgonian (Barremian–Lower Aptian) shelf limestone, with thickness of 5 m on average even if, at places, the bauxite is missing and is replaced by conglomerates. Given the relatively younger age of the bedrock, they must have been deposited over structural or topographic lows as bauxitic detritus, testified by well-bedded clastic bauxite also occurring in the lower part of the deposit.

Type-4: irregular stratiform deposits Located on more or less dolomitic-limestones at the transition between the Purbeckian and Urgonian facies, the Type-1 deposit grades into bauxite with features intermediate between those of Types-1 and 3. The thickness is more variable, due to moderate karstification of the bedrock. At the contact with bedrock, clayey bauxite is almost absent, and high-grade bauxite rests directly on the carbonate substratum. This profile is an intermediate type between residual and detrital profiles that could have been generated when still-evolving lateritic products moved down slope and were redeposited on calcareous bedrock.

The Olmedo mine

Until the 1980s, Sardinian bauxite was poorly known and unexploited. In the 1980s and 1990s, a joint venture aimed to assess the economic potential of the main deposits, triggering new research and exploration and also leading to the opening of a mine close to Olmedo village. During the last 5 years 800,000 tonnes of bauxite were mined, with Al_2O_3 grades as high as 62.5% and SiO_2 about 9% on average. Most of the production derive from underground exploitation. The geometry of the bauxite bed (Fig. 2) allows mining along the dip of the bed using room and pillar excavation. The probable reserves cover an area of 6.5 km^2 and have been estimated at 30 Mt; proven reserves within the area of the mine are 3.8 Mt.

The Olmedo mine is characterized by extensive Type-1 deposits developed on Purbeckian marls. Most of the current production come from Type-1 deposits, the remaining from Type-4 deposits. The Type-1 deposits have a mean thickness of 2 m, and a kaolinite–illite substratum that grades into Fe-rich, oolitic, kaolinitic bauxite. This is overlain by hard oolitic bauxite, with a matrix of illuviated bohemitic material. The upper part of the profile consists of strongly bleached and eluviated bauxite, with a homogeneous weakly oolitic texture. The morphology of the ooids of the Nurra bauxites excludes they have been reworked, similarly to that has been observed for other karst bauxites of the Tethyan area (Mongelli 2002). Some reworked, conglomeratic bauxite, newly enriched in kaolinite, may occur intercalated between this bauxite and the transgressive Coniacian limestone. The Type-4 deposits develop above a more or less dolomitic limestone and differ from the Type-1 for lacking of kaolinite-rich

horizon at the base. Type-4 and Type-1 profiles were sampled by vertical trenches taking into account the different horizons. The representative samples were derived from three different trenches for each profile. The trenches were located along a mine adit, and in a small open pit 500 m east of the mine, respectively. This latter excavation extends over an area as much as 3,000 m^2 in size, where a level of grey kaolinitic clay, bearing centimetre-scale lenses of coal, caps the bauxite.

Methodology

Major element, V, Ni, Cu, Y, Zr and Nb contents have been analysed by XRF on powder pellets, following the matrix correction methods of Franzini et al. (1972, 1975) and Leoni and Saitta (1976). Average errors for trace elements are less than ±5%, except for those elements at concentrations of 10 ppm or lower (±5 to 10%). The estimated precision and accuracy for trace elements determinations are better than 5%, except for those elements having a concentration of 10 ppm and lower (10–15%). Total loss on ignition (LOI) was gravimetrically estimated after overnight heating at 950°C. Cobalt, Cr, Hf, Sc, Th, U, Zn, La, Ce, Nd, Sm, Eu, Tb, Yb and Lu contents were obtained by INAA at Activation Laboratories (Ancaster, Canada). Average errors for these elements range from ±5 to ±20%. Silver, Hg, Ir, Mo, Se and W were usually below the minimum detection limits and will not be considered further in our discussion.

Mineralogical analysis was performed by X-Ray Diffraction, using a Siemens D5000 diffractometer (CuKα radiation, at 40 kV and 30 mA). Scanning electron microscopy and energy-dispersive X-ray spectrometer analyses were carried out on polished sections of bulk rocks using Jeol JSM-5600LV and adjunct Oxford-Inca 200 instrumentation, respectively.

Element 'mobility' has been estimated using an absolute weathering index (Nesbitt 1979), assuming Ti as an immobile element (according to MacLean et al. 1997), and the Upper Continental Crust (UCC; Taylor and McLennan 1985) as parent material. Percent change is expressed as $[(E_{sample}/Ti_{sample})/(E_{UCC}/Ti_{UCC})\text{-}1] \times 100$, where E is the selected element. This index has proved to be reliable in the case of highly weathered materials (Duzgoren-Aydin et al. 2002).

Results

Mineralogy

X-Ray diffraction (XRD) studies on the Nurra bauxites indicate that the porous matrix is composed of kaolinite, boehmite, goethite and anatase, with traces of rutile. The ooids are composed of concentric and irregular shells of alternating boehmite and goethite (and/or hematite). Quartz was only detected in sample 1–7 (from the Type-4 deposit); traces of rutile were detected in almost all samples. The mineral phases identified in the different horizons of the two studied profiles were also quantified (semi-quantitative analysis, ±10%) by XRD. In detail, the Type-4 profile (samples 1-1A to 1-7; Tables 1, 2) shows the following horizons, from the base to the top.

1. A very thin horizon of clayey bauxite, 1–2 cm thick, resting directly on calcareous footwall. The colour is ochre; the mineral assemblage is characterized by abundant kaolinite, boehmite, goethite and anatase (sample 1-1A). This horizon can thicken laterally into clayey, ochre-coloured bauxite, bearing rare reddish ooids in a still relatively clay-rich matrix; the ooids are kaolinite free (sample 1-1B).
2. An oolitic horizon, 30 cm thick, made up of compact ochre-coloured bauxite with boehmite, goethite, anatase and a small quantity of kaolinite.
3. A hardened oolitic bauxite, with rare Fe-rich pisoids. This horizon is 40 cm thick and pale ochre in colour. XRD analyses of the samples reveal an absence of kaolinite and the presence of boehmite, goethite and anatase.
4. A white–pinkish bauxite horizon, 40 cm thick, with rare red goethite pisoids joined to sporadic grey ooids made up of boehmite. Kaolinite is confined only in the joints while anatase is scattered in the matrix.
5. A very hard white, 100 cm thick, bauxite that occupies a level with fine millimetre-scale ooids and sporadic pisoids, both of goethite and boehmite composition. As in the other horizons, XRD analyses confirm the presence of anatase.
6. A laminated, 10 cm thick, horizon of microconglomeratic bauxite due to reworking of the

Table 1 Profile 1 (Type-4 deposit): macroscopic characteristics of the horizons from the base

Horizon	Thickness (cm)	Colour	Ooids–pisoids
1A	1–2	Ochre	–
1B	1–2	Ochre	x
2	30	Ochre	xxx
3	40	Pale ochre	xxx
4	40	White-pinkish	x
5	100	White	xxx
6	10	White	–
7	3	White	–

Table 2 Profile 1 (Type-4 deposit): semi-quantitative mineralogical analyses (wt%)

Horizon	Kaolinite	Boehmite	Goethite	Anatase	Quartz
1A	60.0	18.7	19.0	2.2	–
1B	24.2	51.6	21.4	2.8	–
2	4.6	74.3	17.5	3.5	–
3	-	82.3	14.0	3.7	–
4	14.7	75.8	6.1	3.4	–
5	–	90.5	5.6	3.9	–
6	69.2	23.7	3.3	3.7	–
7	95.0	-	1.7	2.7	0.7

underlying deposit. XRD analyses revealed that this thin layer is enriched in kaolinite and anatase and depleted in boehmite and goethite.

7. A very fine silty, white, 3 cm thick, horizon of resedimented kaolinite bearing small quantities of quartz, anatase and goethite.

The second profile (samples 2-1 to 2-7; Tables 3, 4) pertains to a Type-1 deposit. Starting from the unaltered Purbeckian marls at the base, the following layers have been sampled:

1. Green clays, derived from decarbonation of underlying marls, still containing calcite and composed by illite with minor quantity of kaolinite. The thickness is 50 cm.
2. Reddish–yellow ooidic sample composed of goethite, kaolinite and traces of illite. In this area the thickness of the horizon reaches >100 cm.
3. White–pinkish bauxitic clay dominantly composed of kaolinite and boehmite (Fig. 5), and with sporadic red ooids containing goethite. Titanium is mainly confined to anatase. Thickness is about 30 cm.
4. Red, strongly oolitic, clayey bauxite, with yellow patches of limonite. The main phases are boehmite and kaolinite, in comparable concentrations, followed by goethite and anatase (Fig. 6), which contains the majority of the TiO_2. The abundant ooids are made up of boehmite with minor goethite and hematite. The thickness is about 30 cm.
5. Fine, white–pinkish, ooids-free bauxite; kaolinite and boehmite are the main phases followed by anatase and goethite in similar quantities. The thickness is 80 cm.
6. Fine hardened, aphanitic, white bauxite rich in kaolinite—the main phase, followed by boehmite, anatase and accessory quantities of goethite. The thickness changes rapidly laterally; along the profile it reaches 80 cm.
7. Pink oolitic bauxite with spots of Fe-oxides that fill irregular voids. Large grey pisoids composed of pure boehmite are common. The boehmite content is close to 65%, followed by kaolinite (26%); anatase and goethite each comprise about 4%. The thickness is 50–60 cm.

Table 3 Profile 2 (Type-1 deposit): macroscopic characteristics of the horizons from the base

Horizon	Thickness (cm)	Colour	Ooids–pisoids
1	50	Green	–
2	100	Reddish-yellow	xx
3	30	White-pinkish	x
4	40	Red	xxx
5	80	White-pinkish	–
6	80	White	–
7	50–60	Pink	xx

It should be noted that the 2-7 horizon passes laterally into grey, pyrite-bearing bauxite, the average composition (in wt%) of which is boehmite 66.8%, kaolinite 27.1%, anatase 4.5%, pyrite <1%, goethite <1%. Pyrite occurs either as homogeneously distributed micro-crystals, revealed by SEM/EDS-based observations, or concentrated into spheroidal masses several millimetres in diameter. Other mineral phases were detected by SEM-EDS in different horizons of the two profiles. These include detrital zircon and, in sample 1-2, REE-bearing neo-formed crystals showing

Table 4 Profile 2 (Type-1 deposit): semi-quantitative mineralogical analyses (wt%)

Horizon	Calcite	Illite	Kaolinite	Boehmite	Goethite	Anatase
1	9.6	58.8	23.6	–	6.9	1.1
2	0.9	39.2	41.2	–	17.3	1.2
3	–	–	85.8	9.7	1.9	2.5
4	–	–	42.2	39.2	15.7	3.0
5	–	–	52.3	41.0	3.4	3.4
6	–	–	58.4	36.2	1.7	3.8
7	–	–	26.3	65.4	4.3	4.0

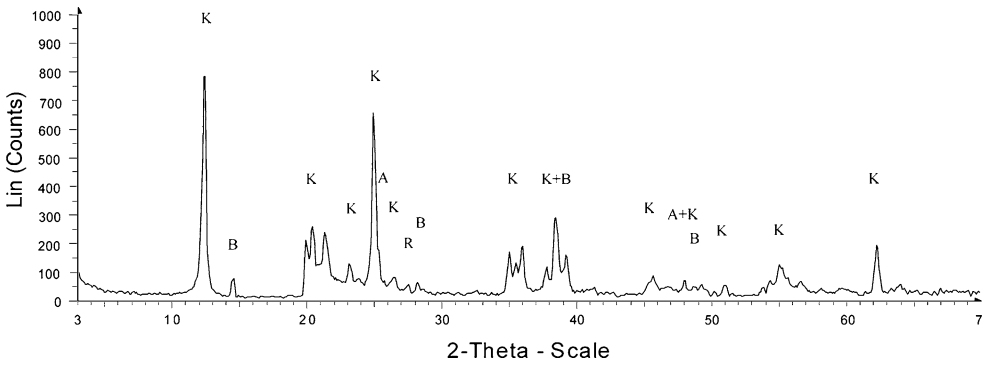

Fig. 5 XRD pattern of sample 2-3 matrix. Legend: *A* anatase. *B* boehmite; *K* kaolinite; *R* rutile

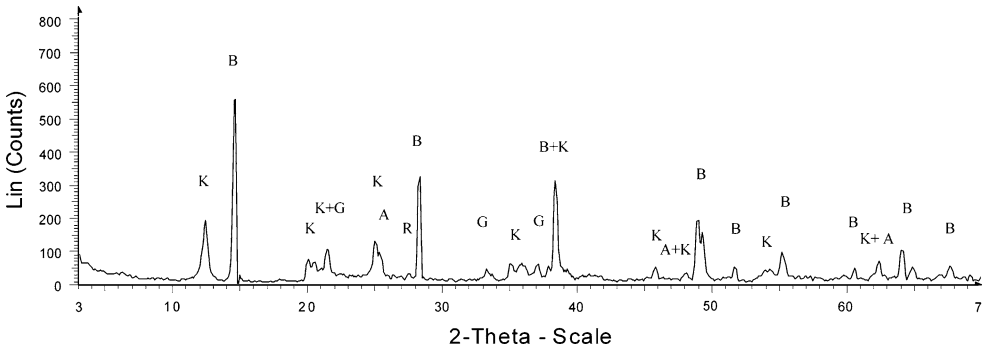

Fig. 6 XRD pattern of sample 2-4. Legend: *A* anatase; *B* boehmite; *G* goethite; *K* kaolinite; *R* rutile

morphological and chemical features (Fig. 7) compatible to some minerals of the bastnäsite group.

Geochemistry

The Al_2O_3, SiO_2, Fe_2O_3, TiO_2 concentrations are the highest among the principal oxides in the analysed samples (Table 5). The SiO_2 content is very high (~40 wt%) in some samples, and can be correlated with the presence of kaolinite. Neoformed kaolinite occurs in late brittle failures, which appear to have exerted a control on the circulation of SiO_2-rich fluids (Oggiano and Mameli 2001). The abundance of kaolinite appears to dilute that of boehmite and, as a result, Al_2O_3 and SiO_2 display a negative correlation (Fig. 8). As expected, TiO_2 correlates positively with Al_2O_3, suggesting that these oxides concentrate in more strongly weathered horizons.

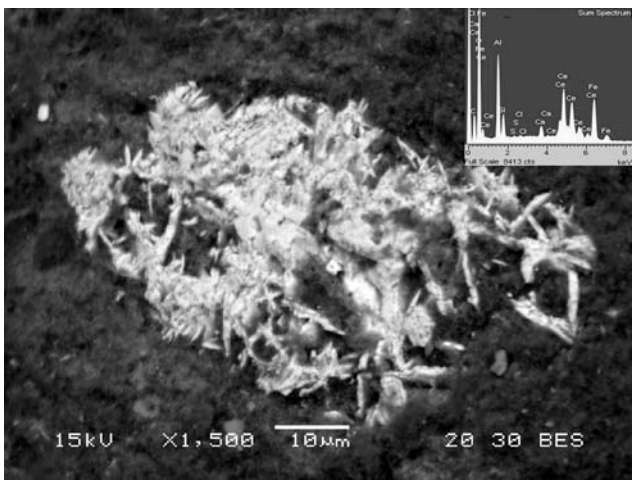

Fig. 7 Back-scattered electron image of the REE-bearing crystals and relative EDX spectra

In the profile developed on the dolomitic limestone (profile 1, Type-4), Fe_2O_3 contents strongly decreases downwards (Fig. 9). In the upper part of the profile, SiO_2 increases, whereas Al_2O_3 decreases. HFSE tend to be conserved whereas the transition elements, with the exception of Ni, decrease upwards. In this profile, there occurs a horizon (1-2), toward the footwall, strongly enriched in LREE and intermediate REE (MREE). In this horizon, however, enrichment of neither Fe nor transition trace elements is observed. In general, a decrease for REE and transition elements is observed upwards. Chondrite-normalized REE patterns of the basal samples, from 1-1A to 1-3 (Fig. 10), have high $\sum$REE contents from 765 to 2,888 ppm, and high $(La/Yb)_{ch}$ $[(La_{sample}/La_{chondrite})/(Yb_{sample}/Yb_{chondrite})]$ ratios (from 7.2 to 27.5; Table 5) and the Eu anomaly ranges from 0.71 to 0.79. Patterns for the upper samples are very similar in shape to samples from the other profile. They have low $\sum$REE (from

Table 5 Major elements, trace elements and ratios distribution in bauxite samples

Sample no.	1-1A	1-1B	1-2	1-3	1-4	1-5	1-6	1–7	2–1	2–2	2–3	2–4	2–5	2–6	2–7
Oxides (wt%)															
SiO_2	27.28	11.01	2.13	ND	6.70	ND	31.38	43.58	42.06	38.97	37.95	19.42	23.92	26.63	12.00
TiO_2	2.18	2.74	3.43	3.65	3.38	3.88	3.62	2.62	1.08	1.22	2.41	2.95	3.34	3.70	3.92
Al_2O_3	38.69	52.15	64.01	68.81	68.86	75.73	46.24	36.43	21.89	25.48	40.06	49.39	54.53	52.70	64.68
Fe_2O3	16.68	18.82	15.53	12.34	5.41	4.94	2.91	1.45	7.14	15.72	1.66	13.92	2.98	1.48	3.79
MnO	0.05	0.05	0.05	0.05	0.04	0.04	0.04	0.04	0.05	0.06	0.04	0.05	0.04	0.04	0.04
MgO	0.42	0.34	0.23	0.21	0.26	0.21	0.38	0.43	2.36	1.62	0.16	0.20	0.20	0.32	0.23
CaO	0.37	0.30	0.19	0.17	0.19	0.16	0.23	0.46	5.32	0.50	0.21	0.21	0.21	0.23	0.20
Na_2O	ND	ND	ND	ND	ND	ND	ND	nd	0.08	0.06	ND	ND	ND	ND	ND
K_2O	0.18	0.08	ND	ND	ND	ND	0.04	0.33	4.05	2.65	0.01	0.06	ND	ND	ND
P_2O_5	0.06	0.05	0.06	0.05	0.03	0.04	0.02	0.03	0.05	0.06	0.04	0.04	0.04	0.03	0.03
LOI (wt%)	14.08	14.46	14.38	14.73	15.13	15.00	15.14	14.64	15.92	13.65	17.46	13.75	14.73	14.88	15.10
Total (wt%)	99.99	100.00	100.01	100.01	100.00	100.00	100.00	100.01	100.00	99.99	100.00	99.99	99.99	100.01	99.99
Trace elements (ppm)															
Sc	59.0	90.2	85.0	69.5	51.4	56.0	61.1	39.0	16.0	26.0	35.3	49.4	36.8	27.3	41.6
V	637	877	822	854	693	750	518	188	141	216	222	499	340	331	449
Cr	474	638	729	848	776	847	715	256	124	177	381	543	498	358	583
Co	66	75	54	47	21	17	18	6	26	74	nd	37	7	nd	5
Ni	215	226	184	150	108	101	277	187	61	119	63	103	86	133	60
Cu	23	29	19	18	nd	nd	nd	nd	7	25	ND	8	ND	ND	ND
Zn	43	51	34	18	7	6	14	14	95	129	11	42	13	12	11
Y	104	143	123	103	66	83	64	55	38	91	45	75	60	57	60
Zr	569	739	793	824	759	948	814	723	260	298	696	773	870	893	951
Nb	50	66	68	69	63	80	74	60	31	32	54	66	72	77	76
Hf	9.5	13.1	14.8	19.0	18.9	19.8	17.5	15.9	4.5	6.9	13.0	16.5	18.6	19.0	21.4
La	209	292	644	148	26	28	15	63	44	133	36	34	23	11	16
Ce	380	585	1470	388	82	60	30	98	68	182	75	89	61	24	34
Nd	131	222	604	175	26	23	11	27	ND	102	26	28	17	9	12
Sm	24.8	44.9	117.0	40.1	7.8	6.9	4.3	4.9	6.6	19.5	4.2	7.0	4.2	2.7	3.4
Eu	5.4	9.8	25.5	8.9	2.2	2.1	1.4	1.3	1.6	4.2	1.1	1.9	1.2	1.1	1.2
Tb	3.0	4.9	9.2	4.0	1.5	1.5	1.3	1.1	1.1	1.9	0.5	1.7	1.0	1.0	1.2
Yb	10.2	15.1	15.8	13.9	10.7	12.3	8.4	6.2	3.4	6.3	4.6	8.4	7.0	6.5	7.1
Lu	1.5	2.3	2.3	2.1	1.6	1.9	1.3	1.0	0.5	1.0	0.7	1.3	1.1	1.0	1.1
Th	22.6	36.5	34.9	49.6	56.0	49.2	35.9	25.7	22.8	23.7	38.0	41.5	55.1	51.9	63.4
U	6.5	9.7	9.1	11.6	10.9	10.6	8.7	5.8	2.3	5.2	6.5	9.1	9.2	13.7	16.2
Ratios															
$(La/Yb)_{ch}$	13.85	13.07	27.54	7.20	1.67	1.53	1.21	6.87	8.69	14.27	5.32	2.76	2.25	1.10	1.48
Ce/Ce*	0.9	0.96	1.06	1.16	1.42	1.02	0.97	0.81	0.76	0.66	1.01	1.23	1.27	1.07	1.05
Eu/Eu*	0.71	0.73	0.79	0.76	0.82	0.85	0.81	0.73	0.73	0.74	0.86	0.73	0.77	0.94	0.83

ND not detected; $(La/Yb)_{ch} = (La/La_{ch})/(Yb/Yb_{ch})$; $Eu/Eu^* = Eu_{ch}/\sqrt{Sm_{ch} \bullet Gd_{ch}}$. Gd_{ch} calculated as $2/3Tb_{ch} + 1/3Sm_{ch}$; $Ce/Ce^* = (3Ce/Ce_{ch})/(2La/La_{ch} + Nd/Nd_{ch})$

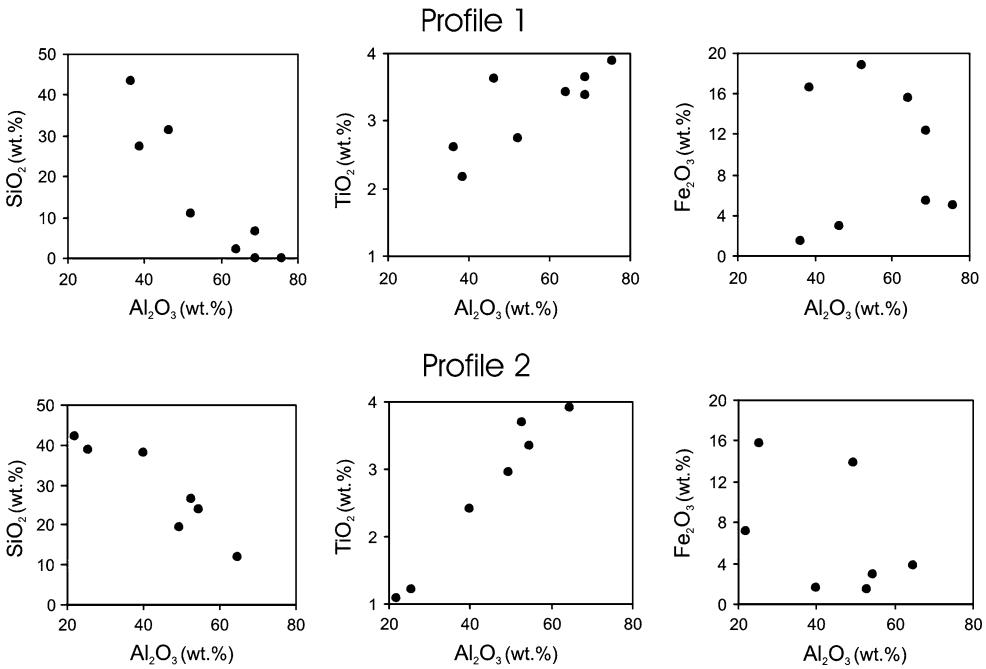

Fig. 8 Binary diagrams showing the correlations between Al_2O_3 and SiO_2, Al_2O_3 and TiO_2, Al_2O_3 and Fe_2O_3 for both profiles. Al_2O_3 and SiO_2 display a negative correlation whereas TiO_2 correlates positively with Al_2O_3, suggesting that these oxides concentrate in more strongly weathered horizons

72 ppm to 202 ppm) and low $(La/Yb)_{ch}$ (from 1.2 to 6.9; Table 5). The Eu anomaly range (0.73 to 0.85) is, however, close to that of the basal samples, and the distribution of the Eu/Eu* ratio all along the profile shows that this index is conservative. The value of the Ce anomaly is generally close to 1 and change in the Ce/Ce* ratio is minor.

In the profile evolving onto a marly Purbeckian bedrock (profile 2, Type-1), SiO_2 and Fe_2O_3 decrease upwards whereas Al_2O_3 is conserved (Fig. 11). HFSE suffer minor changes upwards, likely due to analytical uncertainty, and they may be retained as immobile. LREE and MREE are depleted upwards whereas the transition elements have an erratic distribution, likely related to the distribution of Fe_2O_3. Furthermore, in a horizon in the lower part of the profile, Fe_2O_3 shows enrichment coupled with the enrichment of REE (mostly LREE), Y, U and transition elements (mostly Ni and Co). The chondrite-normalized REE patterns show limited LREE–HREE fractionation (Fig. 12), with the exception of the Fe-rich-sample, and throughout the profile, the $(La/Yb)_{ch}$ ratio decreases upwards (Table 5). The value of the Ce anomaly is generally close to unity, and minor change of the Ce/Ce* ratio is observed throughout the profile. The Eu anomaly is negative (average Eu/Eu* = 0.81 ± 0.08) and the change of the Eu/Eu* ratio is negligible throughout. It should be stressed that $\sum$REE in these samples decreases upwards and it is generally low (from 59 to 156 ppm), if compared to other karst bauxites of the Mediterranean area which have $\sum$REE > 450 ppm (Mongelli 1997). The only exception is represented by the Fe-rich sample which has $\sum$REE = 450 ppm.

Discussion

The bauxitization process

A previous study in the Nurra district suggested that bauxites were formed by weathering of clay-rich debris accumulated onto bedrock (MacLean et al. 1997). The bauxitization proceeded from the surface downwards, with the build-up of residual 'immobile' elements (Al, Ti, HFSE), involving large-scale mobility and ultimate loss of SiO_2 and Fe_2O_3 with increasing Al_2O_3. A similar pattern is observed in the profiles studied in the present work, although some noticeable exceptions have been documented, since both SiO_2 (profile 1) and Fe_2O_3 (profile 2) may increase toward the top of the profiles during and/or after bauxitization.

Regardless of the different types of deposit, epigenetic kaolinite can appear associated with spaced fractures or micro-cracks (Fig. 13a, b), which permitted circulation of SiO_2-rich solutions. These low-pH solutions caused silicification of boehmite, leading to neoformed kaolinite that differs from residual kaolinite by its higher crystallinity (revealed in SEM images; Fig. 14). The SiO_2 addition to the residual rock is well documented and was related to low-temperature

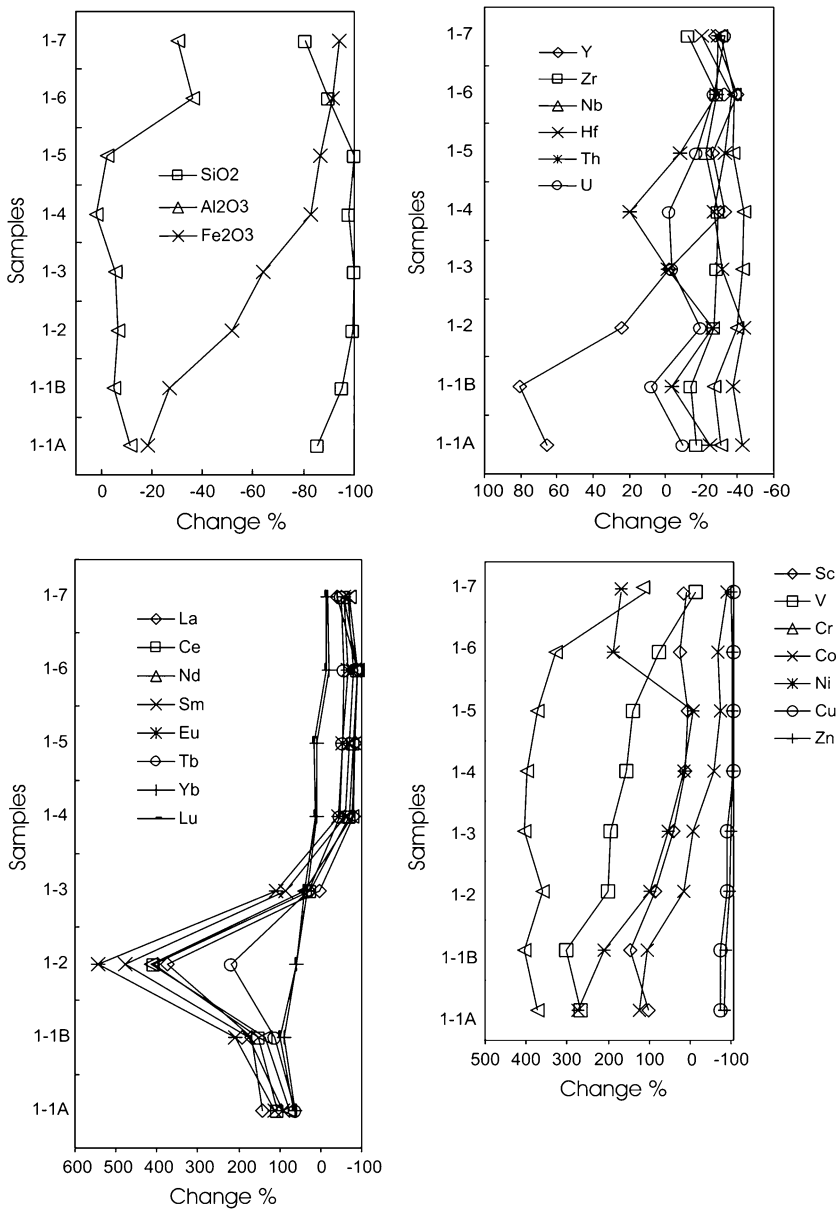

Fig. 9 Mobility of the chemical elements as % change assumes Ti as an immobile element (Profile 1). Fe_2O_3 contents strongly decreases downwards. In the *upper part* of the profile, SiO_2 increases, whereas Al_2O_3 decreases. HFSE tend to be conserved whereas the transition elements, with the exception of Ni, decrease upwards. In this profile, there occurs a horizon (1-2), toward the footwall, strongly enriched in LREE and intermediate REE (MREE). In this horizon, however, enrichment of neither Fe nor transition trace elements is observed. In general, a decrease for REE and transition elements is observed upwards

solutions linked to the Oligocene–Miocene calc-alkaline volcanic activity (Oggiano et al. 1987; Oggiano and Mameli 2001). Close to the Olmedo area such hydrothermal circulation also led to formation of kaolin and bentonite deposits at the expense of pyroclastic and epiclastic protoliths, depending on their pH (Mameli 2001; Cerri and Mameli 2004).

The Fe-rich horizon in profile 2 is goethite-rich, has a typical oolitic texture, and Fe_2O_3 mobility, estimated using the absolute weathering index of Nesbitt (1979), shows a change of +40%. The occurrence of nodular textures associated with Fe accumulation during karst bauxitization in tropical climate conditions is well documented in the Mediterranean area (e.g., Mongelli 1997). Ferruginous ooids result from weathering under tropical climates via a pedogenic mechanism (Nahon et al. 1980). The process consists of Fe concentration into nodular volumes involving migrations from the clay matrix and epigenetic replacement of kaolinite by Fe-oxy-hydroxides. The occurrence and the abundance of Fe-oxy-hydroxides in karst bauxites depend on the absence of conditions which would otherwise promote their stability or inhibit their formation. Oxidation of organic matter favouring local reducing conditions may mobilize Fe as soluble Fe^{2+}. Adsorption by ligands, especially bivalent ones, and an increase in the ionic strength of the soil solution, can both promote goethite instability (Biber et al. 1994).

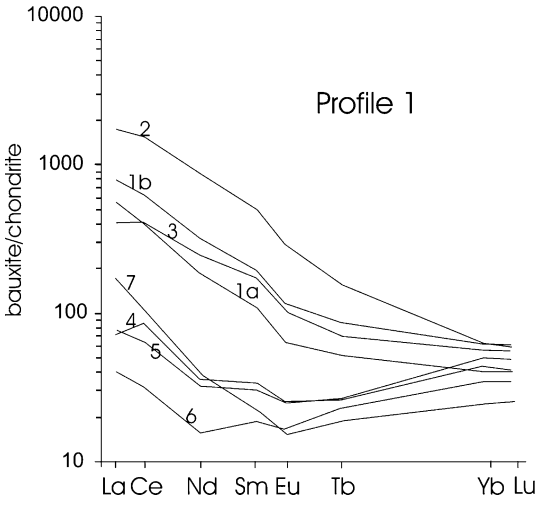

Fig. 10 REE chondrite-normalized patterns (*Profile 1*). Patterns of the basal samples, from 1–1A to 1–3, have high ΣREE contents and high $(La/Yb)_{ch}$ ratios. Patterns for the *upper samples* have low ∑REE and low $(La/Yb)_{ch}$. The distribution of the Eu/Eu* ratio all along the profile shows that this index suffers negligible changes

The pyrite-bearing bauxite brought to light in the open-pit might derive from the reducing activity exerted by bacteria and dead organic matter illuviated into a still porous bauxite from the upper carbonaceous clays during diagenesis. The occurrence of spots of Fe-oxides in horizon 2-7 points to a derivation from the pyrite after late oxidation. In this way, the enrichment of kaolinite in horizons 2-5 and 2-6 can be explained hypothesizing that the derived SO_4^{2-} rich solutions reduced the pH and thus favoured kaolinite stability.

The Fe-rich horizon formed on Purbeckian marl also concentrates some transition elements (Co, Ni, Cr, V) and REE (especially LREE and MREE), a feature observed in other Fe-rich karst bauxites in the Mediterranean area (Mongelli 1997). Goethite exerts an important scavenging action (Künhel 1987) relative to aqueous ions; thus explaining the observed enrichment in transition elements and REE. The $(La/Yb)_{ch}$ ratio is also high in this horizon. Schwertmann and Murad (1983) showed, by long-term experiment, that formation of goethite is pH-dependent and is favoured when the concentration of monovalent Fe^{3+} ions (either $Fe(OH)_2^+$ or $Fe(OH)_4^-$), is at a maximum. The maximum activity for $Fe(OH)_2^+$ is at pH ~4, and that for $Fe(OH)_4^-$ is at pH ~12. However, during karst bauxitization, limestone aquifers play a major role. Such waters are generally close to equilibrium with calcite and have near-neutral to slightly alkaline pH (cf. Appelo and Postma 1993 and references therein). At such pH levels, REE-carbonate complexes prevail (e.g., Johannesson et al. 1995, 1996). The stability of these complexes increases with atomic number, so the preferential retention of HREE in solution as carbonate ions can explain the higher $(La/Yb)_{ch}$ observed in the Fe-rich level. In addition, slight alkaline conditions can favour a preferential adsorption of LREE onto particle surfaces (Sholkovitz 1995). Furthermore, positive correlations exist between Fe_2O_3 and ∑REE ($r = 0.82$, level of significance $\alpha = 0.005$) and between Fe_2O_3 and $(La/Yb)_{ch}$ ($r = 0.76$, level of significance $\alpha = 0.005$) when all samples from both profiles (with the exception of outlayer sample 1-2; discussed subsequently), are considered. This is in agreement with a previous study on karst bauxites from the Mediterranean area (Mongelli 1997), and confirms the first-order importance of Fe-minerals in controlling REE distribution and the shape of chondrite-normalized REE patterns for bauxites.

An exception to this REE-Fe oxy-hydroxides relationship can be envisaged in the Type 4 profile, in which, towards the footwall, a horizon (1-2) which shows Fe_2O_3 depletion has the highest ∑REE abundance (2,888 ppm) and $(La/Yb)_{ch}$ ratio (27.5) among the sample suites of both profiles. Here SEM-EDS study detected a REE-bearing phase (Fig. 7), and it can be confidently assumed that the REE are hosted by accessory minerals. In karst bauxites, the most common accessory REE minerals are fluorocarbonates of the bastnäsite group (Maksimovic and Pantò 1996, and references therein; Mongelli 1997). Strong LREE enrichment is seen in bastnäsite from all deposits in which it occurs (Mariano 1989), and the presence of this mineral can significantly influence the shape of the whole-rock REE pattern. The abundance of the REE phase is too low to allow its identification by XRD alone.

Parental affinity

Most lateritic bauxites can be directly related, through their textures and composition, to the underlying source rocks (e.g., Bardossy and Aleva 1990), but this is rarely the case for bauxites developed above carbonate sequences. A wide range of source rocks have been suggested for karst bauxites, including argillite components of the underlying limestone (as in the case of the Nurra bauxite; MacLean et al. 1997), basement rock debris (Bardossy 1982, and references therein), volcanic ash (Lyew-Ayee 1986; Morelli et al. 2000), and wind-borne material (Pye 1988; Brimhall et al. 1988).

During bauxitization, including the processes resulting in formation of the ores in the Nurra district, fractionation of major, minor and trace elements, including REE, takes place. This may make it difficult

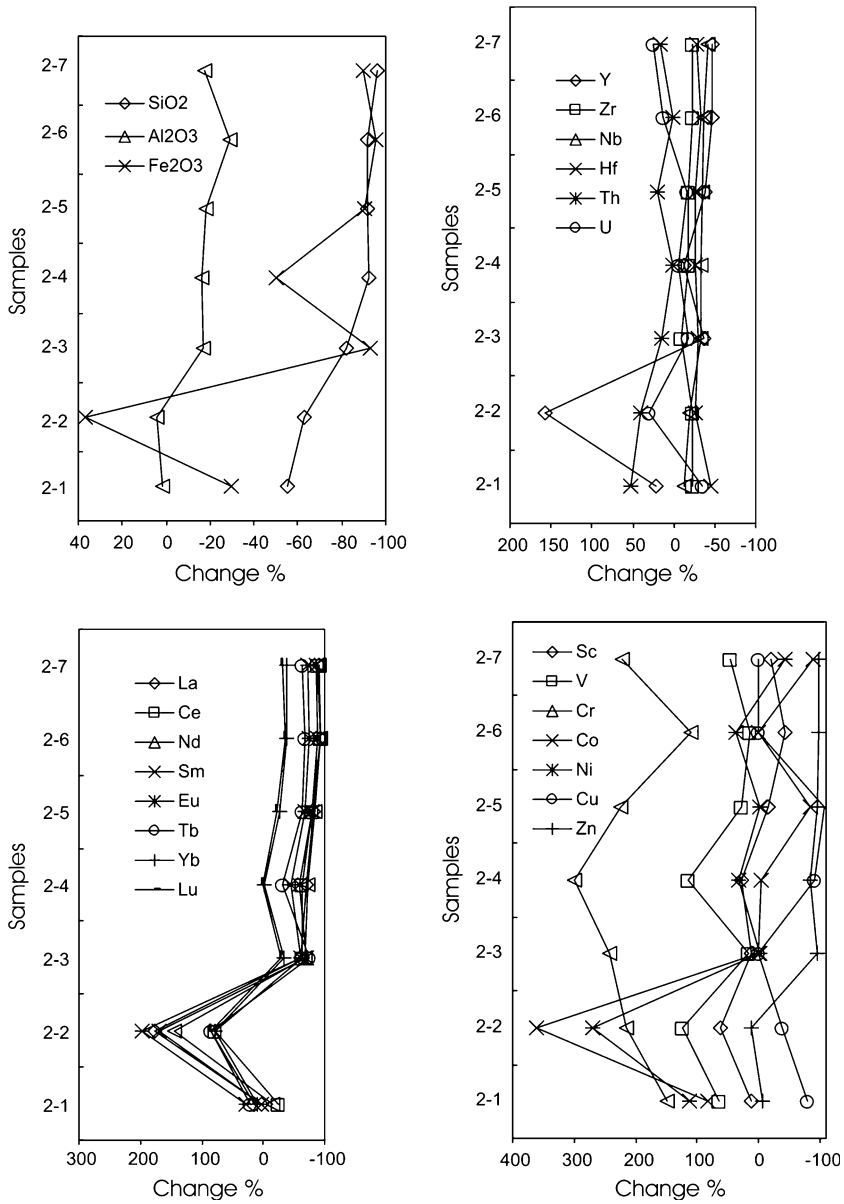

Fig. 11 Mobility of the chemical elements as % change assuming Ti as immobile element (Profile 2). SiO_2 and Fe_2O_3 decrease upwards whereas Al_2O_3 is conserved. HFSE suffer minor changes upwards and they may be retained as immobile. LREE and MREE are depleted upwards whereas the transition elements have an erratic distribution, likely related to the distribution of Fe_2O_3. Furthermore, in a horizon in the lower part of the profile, Fe_2O_3 shows enrichment coupled with the enrichment of REE (mostly LREE), Y, U and transition elements (mostly Ni and Co)

to recognize the source from which the bauxite derives. Some ratios, especially the Eu anomaly, have proved, however, to be retained during intense weathering (e.g., Mongelli 1993), and it should be emphasized that changes in Eu/Eu* are negligible in both profiles. Furthermore it is well known that Al and Ti have a greatest potential for being transferred into the sedimentary rocks, thus preserving a record of protoliths, since they have very low water/upper crust partition coefficients and residence times (e.g., Taylor and McLennan 1985). In addition, Al and Ti were immobile during bauxitization process (see also MacLean et al. 1997) and, as a consequence, we may assume that the TiO_2/Al_2O_3 ratio is a sensitive index of parental affinity. Both Eu/Eu* and TiO_2/Al_2O_3 depart from the average composition of upper crustal rocks and point towards a more mafic composition (Fig. 15a). A similar conclusion is reached using the Ti/Cr ratio, although more caution is needed due to the moderate reduction in Cr content observed at the top of the profile 1. In general, however, the Nurra bauxites have Ti/Cr values decisively lower than those of the UCC (Fig. 15b), further supporting a mafic source for the argillaceous sediments (MacLean et al. 1997) from which the bauxite has formed. Mafic rocks are well represented in the Hercynian basement of western Sardinia (Di Pisa et al. 1992). They have been exposed during middle Cretaceous erosive phase further northwest of Monte la Campana where, not only the Malm strata, but also the entire pre-upper Cretaceous sequence could have

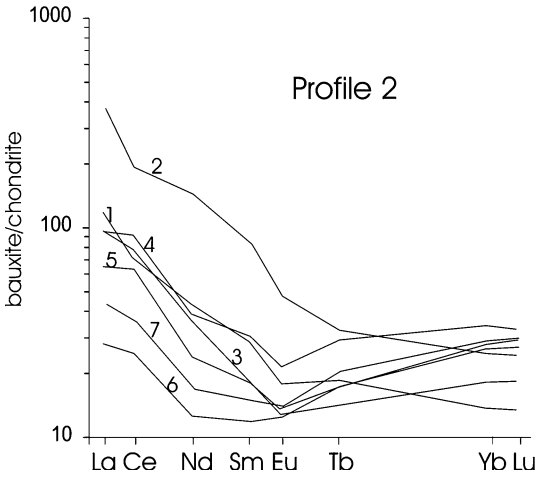

Fig. 12 REE chondrite-normalized patterns (*Profile 2*). Patterns show limited LREE–HREE fractionation, with the exception of the Fe-rich-sample, and throughout the profile, the $(La/Yb)_{ch}$ ratio decreases upwards. The $\sum$REE in these samples decreases upwards and it is generally low, if compared to other karst bauxites of the Mediterranean area which have $\sum$REE > 450 ppm (Mongelli 1997). The only exception is represented by the Fe-rich sample which has $\sum$REE = 450 ppm

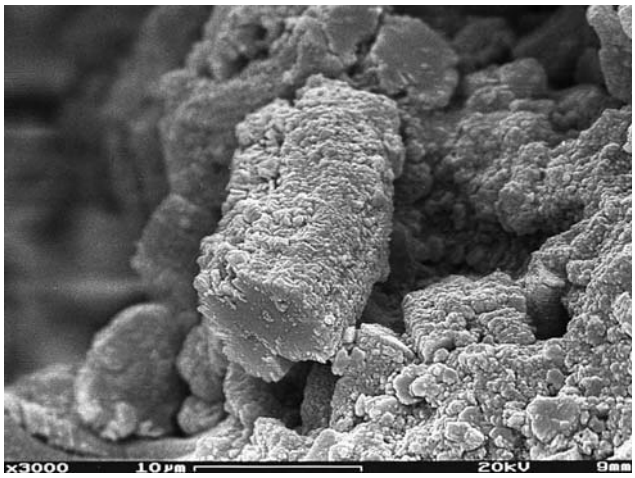

Fig. 14 Secondary electron image showing coarse, thick stacks of kaolinite crystals growing on the walls of the fracture shown in Fig. 13

been eroded in correspondence of some structural high.

Finally, it has to be noted that both profiles, in spite of their different features, share, broadly speaking, very similar values of Eu/Eu*, TiO_2/Al_2O_3 and Ti/Cr, suggesting they have a similar parental affinities.

Summary

Texture is a first-order factor controlling the chemical and mineralogical features of the Nurra bauxites. The bauxites are composed mainly of Al, Si, Fe and Ti, hosted by boehmite, goethite, kaolinite and anatase, with minor hematite and rutile. In the matrix, in addition to Al- and Fe-oxy-hydroxides, kaolinite and Ti-oxides occur, whereas ooids are exclusively made of Al and Fe oxy-hydroxides. The formation of epigenetic kaolinite was promoted by circulation of low-temperature hydrothermal solutions associated with calc-alkaline volcanic activity, and favoured by the occurrence of fractures and fissures, caused Si addition to the residual rock.

Ferruginous ooids can result from Fe migration from the matrix that replaced kaolinite. Formation of Fe oxy-hydroxides depends on a number of factors, including changes of the water activity in the pedogenic environment (e.g., Tardy and Nahon 1985) and may reflect climatic fluctuations (e.g., Mongelli 2002). The Fe-rich horizons of bauxite concentrate REE and especially LREE, in addition to first-row transition elements; likely because of the significant scavenging action exerted by goethite. REE-enrichment is not observed in boehmite-rich levels that have very low REE contents. Very high REE contents are observed in a Fe-depleted level, due to the occurrence of REE accessory minerals, probably of the bastnäsite group.

Conservative indices, including TiO_2/Al_2O_3 and Ti/Cr ratios and the Eu anomaly, suggest that beds from which the bauxites formed are derived from mafic rocks of the Variscan basement of western Sardinia.

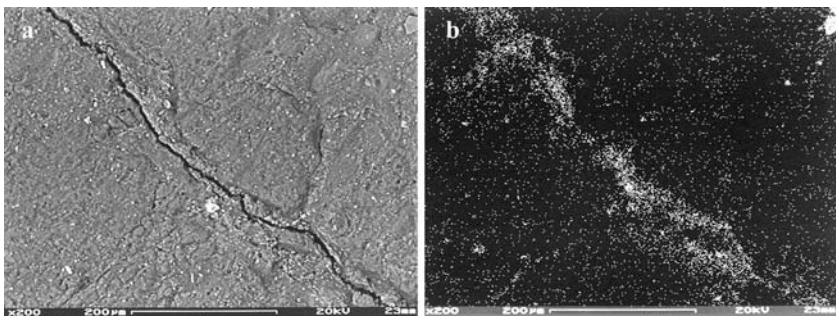

Fig. 13 Back-scattered electron image showing an open microfracture in compact bauxite (sample 1-4) and X-ray map showing the distribution of Si around the fracture

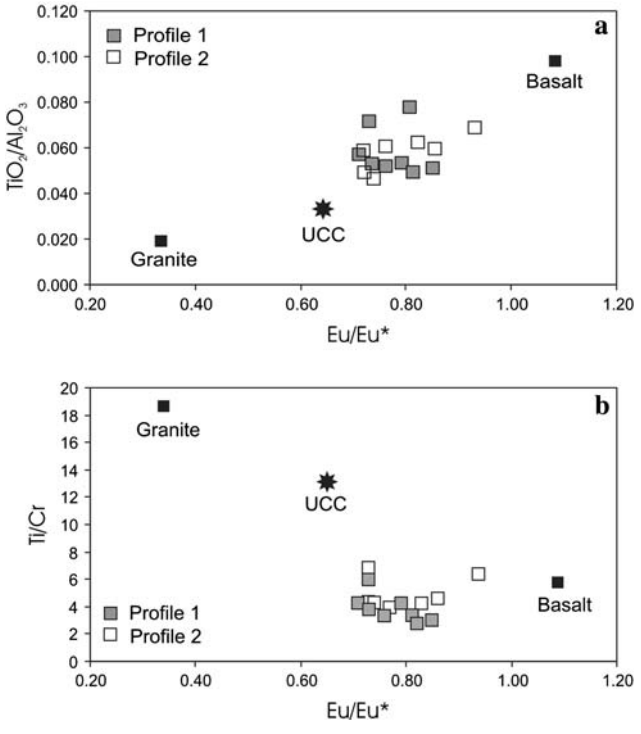

Fig. 15 Eu-anomaly vs TiO_2/Al_2O_3 (**a**) and vs Ti/Cr (**b**) diagrams. Eu/Eu* and TiO_2/Al_2O_3 depart from the average composition of upper crustal rocks and point towards a more mafic composition. A similar conclusion is reached using the Ti/Cr ratio. In general, the Nurra bauxites have Ti/Cr values decisively lower than those of the UCC, further supporting a mafic source for the argillaceous sediments (MacLean et al. 1997) from which the bauxite has formed

This implies that the Variscan basement was exhumed and eroded during the middle Cretaceous.

Acknowledgments We thank Sardabauxiti for their logistic support and access to the Olmedo mine and also Igor M. Villa and an anonymous referee for precious comments and review. This study was financially supported by a grant from Fondazione Banco di Sardegna.

References

Appelo CAJ, Postma D (1993) Geochemistry, groundwater and pollution. Balkema, Rotterdam, pp 1–536

Bardossy G (1982) Karst bauxites, bauxite deposits on carbonate rocks. In: Developments in economic geology, vol 14. Elsevier, Amsterdam, pp 1–441

Bardossy G, Aleva GJJ (1990) Lateritic bauxites. In: Developments in economic geology, vol 27. Elsevier, Amsterdam, pp 1–624

Biber MV, Dos Santos A, Stumm W (1994) The coordination chemistry of weathering: IV. Inhibition of the dissolution of oxide minerals. Geochimica et Cosmochimica Acta 58:1999–2010

Brimhall GH, Lewis CJ, Ague JJ, Dietrich WE, Hampel J, Rix P (1988) Metal enrichment in bauxites by deposition of chemically mature aeolian dust. Nature 333:819–824

Cerri G, Mameli P (2004) Secondary mineral assemblages within epiclastites of western Logudoro, Sardinia, Italy. 56th Rocky Mountains and 100th Cordilleran Sections Meeting. The Geological Society of America, Boulder (Colorado) 36-IV:81

Cherchi A, Schroeder R (1976) Rinvenimento di Cenomaniano superiore a ''Alveolinidae'' in Sardegna e sue affinità paleobiogeografiche. Rendiconti Accademia Nazionale dei Lincei 59:800–807

Combes PJ (1972) Les différentes types de bauxites sur substratum carbonaté dans le Languedoc et l'Ariége. Remarques sur la notion d'allochtonie et d'autochtonie. Comptes Rendus de l'Académie des Sciences 274:1613–1616

Combes PJ (1990) Typologie, cadre géodynamique et genèse des bauxites françaises. Geodinamica Acta 4:91–109

Combes PJ, Oggiano G, Temussi I (1993) Geodynamique des bauxites sardes, typologie, génese et controle paleotectonique. Comptes Rendus de l'Académie des Sciences Sèrie II 316:403–409

Dercourt J, Zonenshain LP, Ricou LE, Kazmin VG, Le Pichon X, Knipper AL, Grandjacquet C, Sborshchikov IM, Boulin J, Sorokhtin O, Geyssant J, Lepvrier C, Bijy-Duval B, Sibuet JC, Savostin LA, Westphal M, Lauer JO (1985) Présentation de 9 cartes paléogéographiques au 1:20.000.000 s'étendant de l'Atlantique au Pamir pour la période du Lias à l'Actuel. Bulletin Société Géologique de France 5:637–652

Di Pisa A, Gattiglio M, Oggiano G (1992) Pre-Hercynian magmatic activity in the Nappe Zone (internal and external) of Sardinia: evidence of two within-plate basaltic cycles. IGCP Project 276 Newslett 5:33–44

Duzgoren-Aydin NS, Aydin A, Malpas J (2002) Re-assessment of chemical weathering indices: case study on pyroclastic rocks of Hong Kong. Eng Geol 63:99–119

Fenner J (2001) Middle and Late Albian geography, oceanography, and climate and the setting of the Kirchrode I and II borehole sites. Palaeogeogr Palaeoclimatol Palaeoecol 174:5–32

Frakes LA (1979) Climates throughout geologic time. Elsevier, Amsterdam, pp 1–310

Frakes LA (1986) Mesozoic–Cenozoic climatic history and causes of the glaciation. In: Hsü KJ (ed), Mesozoic and cenozoic oceans. AGU Geodynamic Series 15:33–48

Franzini M, Leoni L, Saitta M (1972) A simple method to evaluate the matrix effects in X-ray fluorescence analysis. X-Ray Spectrom 1:151–154

Franzini M, Leoni L, Saitta M (1975) Revisione di una metodologia analitica di fluorescenza-X basata sulla correzione completa degli effetti di matrice. Rendiconti Società Italiana di Mineralogia e Petrologia 31:365–378

Herrle JO, Pross J, Friedrich O, Köβler P, Hemleben C (2003) Forcing mechanisms for mid-Cretaceous black shale formation: evidence from the Upper Aptian and Lower Albian of the Vocontian Basin (SE France). Palaeogeogr Palaeoclimatol Palaeoecol 190:399–426

Johannesson KH, Lyons WB, Stetzenbach KJ, Byrne RH (1995) The solubility control of rare earth elements in natural terrestrial waters and the significance of PO_4^{3-} and CO_3^{2-} in limiting dissolved rare earth concentrations: a review of recent information. Aquat Geochem 1:157–173

Johannesson KH, Stetzenbach KJ, Hodge VF, Lyons WB (1996) Rare earth element complexation behavior in circumneutral pH groundwaters: assessing the role of carbonate and phosphate ions. Earth Planet Sci Lett 139:305–319

Künhel RA (1987) The role of cationic and anionic scavengers in laterites. Chem Geol 60:31–40

Laville P (1981) La formation bauxitique provençale (France). Séquence des faciès chimiques et paléomorphologie crétacèe. Chronique de la Recherche Minière 461:51–68

Leoni L, Saitta M (1976) Determination of yttrium and niobium on standard silicate rocks by X-ray fluorescence analysis. X-Ray Spectrom 5:29–30

Lyew-Ayee PA (1986) A case for the volcanic origin of Jamaican bauxites. Proceedingsof the VI Bauxite Symposium 1986. J Geol Soc Jam 1:9–39

MacLean WH, Bonavia FF, Sanna G (1997) Argillite debris converted to bauxite during karst weathering: evidence from immobile element geochemistry at the Olmedo Deposit, Sardinia. Mineralium Deposita 32:607–616

Mameli P (2001) Occurrence of halite in kaolin of NW Sardinia: genetic implications. In: Cidu R (ed) Water–rock interaction. Balkema, Lisse, pp 729–733

Maksimovic ZJ, Pantò G (1991) Contribution to the geochemistry of the rare earth elements in the karst-bauxites deposits of Yugoslavia and Greece. Geoderma 51:93–109

Maksimovic ZJ, Pantò G (1996) Authigenic rare earth minerals in karst-bauxites and karstic nickel deposits. In: Jones AP, Wall F, Williams CT (eds) Rare earth minerals: chemistry, origin and ore deposits. The Mineralogical Society Series 7, pp 257–280

Mariano AN (1989) Economic geology of rare earth elements. In: Geochemistry and mineralogy of rare earth elements. Rev Mineral 21:309–337

Mongelli G (1993) REE and other trace elements in a granitic weathering profile from ''Serre'', southern Italy. Chem Geol 103:17–25

Mongelli G (1997) Ce-anomalies in the textural components of Upper Cretaceous karst bauxites from the Apulian Carbonate platform (southern Italy). Chem Geol 140:69–79

Mongelli G (2002) Growth of hematite and boehmite in concretions from ancient karst bauxite: clue for past climate. Catena 50:43–51

Morelli F, Cullers R, Laviano R, Mongelli G (2000) Geochemistry and palaeoenvironmental significance of Upper Cretaceous clay-rich beds from the Peri-adriatic Apulia carbonate platform, southern Italy. Periodico di Mineralogia 69(2):165–183

Nahon D, Carozzi AV, Parron C (1980) Lateritic weathering as a mechanism for the generation of ferruginous ooids. J Sediment Petrol 50:1287–1298

Nesbitt HW (1979) Mobility and fractionation of rare earth elements during weathering of a granodiorite. Nature 279:206–210

Oggiano G, Sanna G, Temussi I (1987) Caractères geologiques, gitologiques et geochemiques de la bauxite de la Nurra. In: Cherchi A (eds) Livret-Guide excursion en Sardaigne 24–29 Mai 1987. Groupe Francais du Crétacé, Cagliari, pp 72–124

Oggiano G, Mameli P (2001) The bauxite of North-Western Sardinia. Rendiconti della Facoltà di Scienze MM.FF.NN. dell'Università di Cagliari 71(II):59–73

Pecorini G (1965) Stratigrafia e distribuzione delle bauxiti della Nurra (Sardegna Nord Occidentale). Symposium Associazione Mineraria Sarda 1:1–15

Pecorini G (1969) Le Clavatoracee del ''Purbeckiano'' di Cala d'Inferno nella Nurra di Alghero (Sardegna Nord Occidentale). Bollettino della Società Sarda di Scienze Naturali 5:1–14

Pye K (1988) Bauxites gathering dust. Nature 333:300–301

Puigdefabregas C, Souquet P (1986) Tecto-sedimentary cycles and depositional sequences of the Mesozoic and Tertiary from the Pyrenees. Tectonophysics 129:173–203

Rousset C (1969) Le bombement varois: relation entre la bauxitisation au Crétacé moyen en Provence et l'évolution régionale de région en régime karstique. Comptes Rendus de l'Académie des Sciences 268:2331–2334

Schwertmann U, Murad E (1983) Effect of pH on the formation of goethite and hematite from ferrihydrite. Clays Clay Miner 31:277–284

Sholkovitz ER (1995) The aquatic chemistry of rare earth elements in rivers and estuaries. Aquat Geochem 1:1–34

Taylor SR, McLennan SM (1985) The continental crust: its composition and evolution. Blackwell, Oxford, pp 1–312

Tardy Y, Nahon DB (1985) Geochemistry of laterites. Stability of Al-goethite, Al-hematite and Fe^{3+}-kaolinite in bauxites and ferricretes. An approach to the mechanism of concretion formation. Am J Sci 285:865–903

Vigliotti L, Langenheim VE (1995) When did Sardinia stop rotating? New paleomagnetic results. Terra Nova 7:424–435